CO4-1 Millimeter Wave Absorption Spectra of Ionic Liquids

T. Awano and T. Takahashi[1]

Faculty of Engineering, Tohoku Gakuin University
[1]Research Reactor Institute, Kyoto University

INTRODUCTION: Ionic liquid (IL) is molten salt at room temperature. It is interesting to compare ionic motion in ionic liquids with those in superionic conductor.

We have observed millimeter wave absorption bands around 6 and 8 cm^{-1} in AgI-superionic conductive glasses. These bands were also observed in CuI-superionic ones[1-3]. These bands seems to be due to collective motion of conductive ions because of their frequency, although how conduction ions moves in correlation is not clear.

Recently, we have observed sub-terahertz absorption bands of ILs[4,5]. These bands seems to be due to ionic movement because of their temperature dependence. That is to say, the absorption disappear at low temperatures at which the IL is solid. However, the thermal change of these bands were in various way. This difference seems to be due to the difference of their phase transition to the solid states (crystal or glass).

In this study we have measured millimeter wave absorption spectra of 33 ILs to make clear the ionic movement from the temperature change of absorption spectra.

EXPERIMENTS: A fixed amount of ionic liquids (Tokyo Chemical Industry Co., Ltd.) were spread into filter paper. Transmission spectra of single and double papers with ionic liquids were measured at room temperature and low temperatures. Absorption spectra were obtained by subtraction of them.

RESULTS: Three types of the spectral change occurred at temperature above melting point or glass transition temperature[5]. The absorption bands in the ILs which are crystal in the solid state showed rapid decrease at their melting points[4]. On the other hand, those in ILs which are vitreous in the solid state weakened and shifted gradually. Others showed complicated change as shown in Figs. 1 and 2.

Fig. 1 shows absorption spectra of Triethylsulfonium bis(trifluoromethane)sulfonimide([TES][TFSI]). Figs. 1 and 2 shows increment spectra from that at 88K. At this temperature, these ILs are solid and have only little absorption in this spectral range. At 158K, all four absorption bands decreased below the baseline.

Fig. 2 shows absorption spectra of Tributyl(2-methyloxyethyl)-phosphonium bis(trifluoromethane)sulfonimide([TBMOEP][TFSI]). The 9.5 cm^{-1} band decreased below the baseline at 158 K.

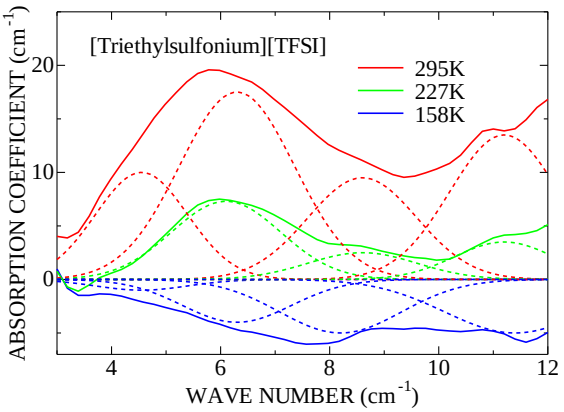

Fig. 1. Absorption increment spectra of [TES][TFSI]. The baseline is the absorption spectrum at 88 K.

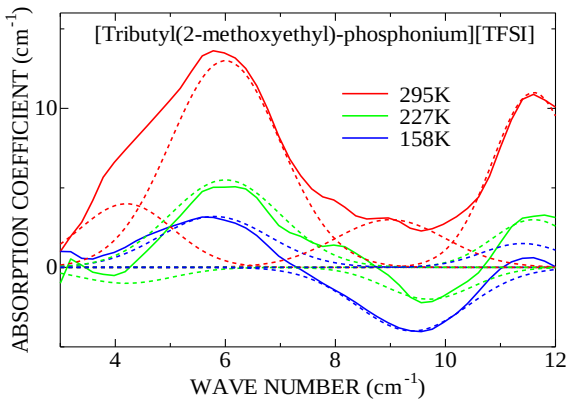

Fig. 2. Absorption increment spectra of [TBMOEP][TFSI]. The baseline is the absorption spectrum at 88 K.

REFERENCES:

[1] T. Awano and T. Takahashi, J. Phys. Conf., **148** (2009) 012040/1-4.
[2] T. Awano and T. Takahashi, J. Phys. Soc. Jpn. **79** Suppl. A (2010) 118-121.
[3] T. Awano and T. Takahashi, Proceedings of the 13th Asian Conference on Solid State Ionics, (2012) 569-576.
[4] T. Awano and T. Takahashi, KURRI Progress Report 2014, CO4-2.
[5] T. Awano , A. Shikoda and T. Takahashi, 20th International Conference on Solid State Ionics, (2015) D2.02.

CO4-2 Synthesis of Metal Nanoparticles and Nanocomposites by Gamma-ray Irradiation Reduction Method

F. Hori, H. Nakanishi, A. Tokai, M. Tanaka, A. Iwase, K. Okitsu, Y. Mizukoshi[1] and M. Sakamoto[2]

Dept. of Mater. Sci., Osaka Prefecture University

[1]*Institute of Materials Research, Tohoku University*
[2]*Research Reactor Institute, Kyoto University*

INTRODUCTION: Metallic nanoparticles have some specific properties, which are not appeared in bulk materials such as catalytic activities, magnetic properties, electro conductivity and light absorption. These properties depend on its size, shape, structure, chemical composition and so on. They have many possibilities to applied for various industrial fields. Generally, many kinds of metal nanoparticles commercially are synthesized by using chemical reaction method. Recent years, some reports show that it is possible to fabricate various metal nanoparticles under irradiation reduction fields such as ultrasonic, electron beam, ion beam and gamma-ray irradiation. So far, we have reported that synthesis of shape and size controlled Au, Pd, Pt, Cu and these complex nanoparticles by these reaction fields. On the other hand, it is possible that graphene with Pt nanocomposits have high catalytic activity and selectivity due to their excellent properties of graphene and Pt nanoparticles. We have developed a one-step gamma-ray irradiation method to synthesize nanocomposites composed of graphene and Pt nanoparticles from aqueous solution containing graphene and Pt ions in water [1].

EXPERIMENTS: Aqueous solutions with a given concentration of Hydrogen hexachloroplatinate (IV) hexahydrate ($H_2PtCl_66H_2O$, Pt(IV)), SDS or 2-propanol. Graphenepowder (6 - 8 nm thick x 5 μm wide) was added into this water solution. The solution was argon gas purged and sealed into polystyrene vessels. After dispersion by an ultrasonic cleaning bath, they were irradiated at about 300 K with γ-rays from ^{60}Co radio active source at gamma irradiation facility in KURRI, Kyoto University. The total dose was fixed to 10 kGy with dose rate of 15 kGy/h. After irradiation, the products were separated by centrifugation, washed with water and dried by freeze-drying. UV–vis absorption spectra were measured and all products were observed by conventional TEM. Infrared spectra and Raman spectra (RS) of the prepared samples were collected by a Fourier-transform infrared spectro-photometer (FT-IR) and a Raman spectrophotometer.

RESULTS:
Figure 1 shows the UV/vis absorption spectra for aqueous solutions before and after gamma-ray irradiation. The absorption peak around 260 nm, which shows Pt complex ions, disappears after γ-ray irradiation. This shows that Pt complex ions were reduced by γ-ray induced reductive radicals such as hydrated electron (e_{aq}^-) and hydrogen radicals. Figure 2 shows the TEM images of Pt and graphene solution sample including SDS and 2-propanol as an additive after γ-ray irradiation. Pt nanoparticles homogeneously supported on graphene were formed. The avarage size of Pt nanoparticles was about 30 nm. On the other hand, from the results of FT-IR and RS experiments, it was confirmed that graphene surface was chemically modified by the carbonil groups formed after irradiation. Consequently, fabricated Pt nanoparticles under γ-ray irradiation field were supported on the surface modified graphene.

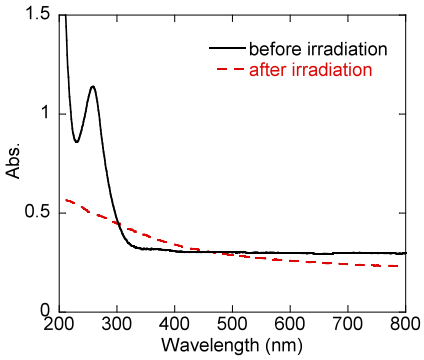

Fig. 1 UV/vis absorption spectra of aqueous solutions of Pt and graphene before and after gamma-ray irradiation.

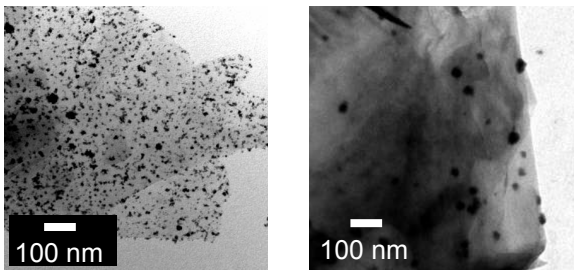

Fig. 2 TEM images of Pt nanoparticles supported on graphene surface synthesized by gamma-ray irradiation.

References

[1] A.Tokai, K.Okitsu, F.Hori, Y.Mizukoshi, A.Iwase, Rad. Phys. Chem. 123, (2016) 68-72

CO4-3

Gamma-ray Induced Photocurrent of Field Emitter Array and Cadmium Telluride-Cadmium Sulfied Photodiode

Y. Gotoh, H. Tsuji, M. Nagao[1], T. Okamoto[2], N. Sato[3], T. Masuzawa[4], Y. Neo[4], H. Mimura[4], M. Akiyoshi[5] and I. Takagi

Graduate School of Engineering, Kyoto University
[1]Nanoelectronics Research Institute, National Institute of Advanced Industrial Science and Technology
[2]National Institute of Technology, Kisarazu College
[3]Research Reactor Institute, Kyoto University
[4]Research Institute of Electronics, Shizuoka University
[5]Radiation Research Center, Osaka Prefecture University

INTRODUCTION: Vacuum image sensors with the combination of a field emitter array (FEA) and a photodiode are possible candidate as an elemental part of the camera for observation of interior of the pressure vessel of Fukushima nuclear power plant, the 1st [1]. We have been investigating the deterioration of the performance of FEA and cadmium telluride-cadmium sulfide (CdTe/CdS) photodiode since 2014. These elements already exhibited sufficient endurance against γ-ray irradiation up to 200 kGy. However, the tests have been done after the γ-ray irradiation, and therefore little information on the change in the property under γ-ray irradiation was obtained. There exist many phenomena associated with the γ-ray irradiation, including generation of photocurrent, which prevent us from detecting image signal. This report describes the results of the measurements of photocurrent of FEA and photodiode.

EXPERIMENTS: Six FEAs with different sizes including those of which side length is either 40 or 60 μm were mounted on a single chip. Each FEA possessed a focus electrode in addition to the emitter and the gate [2]. Each FEA has the insulating layer between the emitter and the gate, and also between the gate and the focus electrode. The chip was mounted on the 28-pin LSI package, and was installed in a vacuum vessel. The CdTe and CdS films were prepared by close space sublimation technique and CVD [3]. Gamma-ray irradiation was performed at Gamma-ray Irradiation Facility, Research Reactor Institute, Kyoto University. Current-voltage (*I-V*) characteristics of the FEAs and the photodiodes were measured during irradiation of γ-ray. The irradiations were done at 20, 30, and 40 cm from the radiation source to check the dose rate dependence. The absorbed doses at 20 and 40 cm were 1.58 and 0.33 kGy h^{-1}, respectively.

RESULTS: Fig. 1 shows the *I-V* characteristics of the photodiode; dashed line, solid line, and dotted line show the dark current, the current during γ-ray irradiation, and the current with visible light at 20 cm apart from the γ-ray source. The photocurrent due to the γ-ray irradiation was almost proportional to the dose rate and as large as 400-500 nA at the bias of -10 V under the absorbed dose rate of 1.58 kGy h^{-1}. Fig. 2 shows the *I-V* characteristics of the 60 μm-FEA. For the 40 μm-FEA, similar behavior was observed. In this case, both emitter current I_E and gate current I_G were measured individually. The bias was given only to the emitter. Without γ-ray irradiation, both I_E and I_G were almost zero. With γ-ray irradiation, I_E and I_G showed linear increases with applied voltage. However, the I_G did not meet with the I_E. The reason for this has not yet been clarified. Since the irradiation tests were performed within a limited time of 5-10 min for each condition, no degradation of the samples were observed after the irradiation. Separately performed experiments revealed that the FEA and the photodiodes had sufficient tolerance up to 1.2 MGy.

ACKNOWLEDGMENTS: A part of this study is the result of "Development of radiation tolerant compact image sensor with a field emitter array", carried out under the Center of World Intelligence Project for Nuclear S&T and Human Resource Development by the Ministry of Education, Culture, Sports, Science and Technology of Japan.

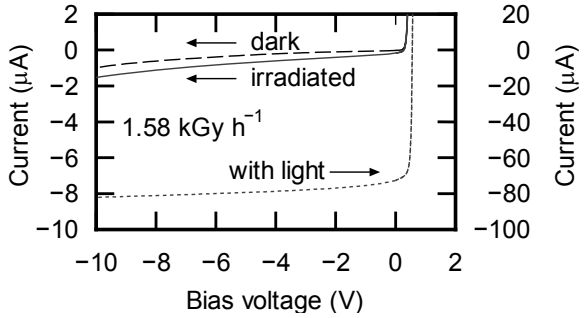

Fig. 1. *I-V* characteristics of CdTe/CdS photodiode with and without γ-ray irradiation.

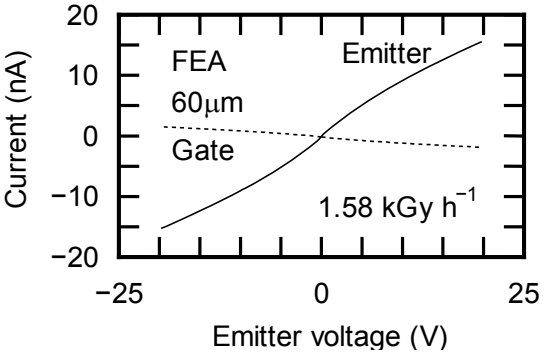

Fig. 2. *I-V* characteristics of FEA under γ-ray irradiation.

REFERENCES:

[1] Y. Gotoh *et al.*, 28th Int'l Vacuum Nanoelectronics Conference, Guangzhou, China, July, 2015, p.240.
[2] M. Nagao *et al.*, J. Vac. Sci. Technol. B **34** (2016) 02G108/1-6.
[3] T. Okamoto *et al.*, Jpn. J. Appl. Phys. **52** (2013) 102301/1-3.

CO4-4 The Development of AMOC System for KUR Positron Beam Facility

K. Nagumo, Y. Nagai, K. Inoue, T. Toyama, Y. Shimizu, B. Han, M. Shimodaira, A. Kinomura[1], T. Yoshiie[1], Q. Xu[1]

Institute for Materials Research, Tohoku University,
[1]Research Reactor Institute, Kyoto University

INTRODUCTION: Low-energy antiparticles are becoming increasingly important for both scientific and technological applications. In particular, positrons offer new ways to study a wide range of phenomena including scattering with atoms and molecules, the Fermi surface of metal, and defects and ultrafine precipitates in solids.

The ultrafine precipitation of Cu impurities contained in the old light water reactor pressure vessel (RPV) steels are considered to be one of the main origins for the embrittlement of old RPV. The formation of these ultrafine Cu precipitates is enhanced by the neutron irradiation. This mechanism of embrittlement is one of the topical issues for safety operation of reactors in the field of nuclear industry.

Positron annihilation spectroscopy is one of the powerful tools for detecting sensitively the vacancy type defects in metals and positron affinity precipitates such as the ultrafine Cu precipitates in Fe. In order to investigate the correlation between the formation of the Cu precipitates and the defect clusters induced by neutron irradiation, the technique of the positron age-momentum correlation (AMOC) using high intensity slow positron beam is required. Then, we are constructing a new positron beam facility with high positron intensity at the Kyoto University Research Reactor (KUR), which is the first reactor based positron beam in Japan [1]. The first slow positron beam was successfully obtained from B1-hole at KUR two years ago [2]. Since then, the KUR operation have been stopped. In this work, the AMOC system that conforms to the measurement using KUR positron beam facility was developed during the reactor shutdown.

EXPERIMENTS and RESULTS: AMOC is a technique that allows direct observation of the time dependent transitions of the positron states through simultaneous measurements of both the lifetime and the momentum distributions of annihilating electron-positron pairs. In case of the conventional 3-gamma coincidence system that employ Na-22 for positron source, one nuclear gamma ray of 1.275MeV is used for time determination of positron creation, and two annihilation gamma rays are used for time determination of positron annihilation and measuring momentum distribution of electron-positron pair. In case of the measurements using KUR positron beam, the start signal should be acquired from pulsing trigger of buncher unit instead nuclear gamma ray, which can convert the continuous positron beam from the reactor into a pulsed beam, as shown in Figure 1. The coincidence module is consisted of Fast Amplifier, Timing Filter Amplifier, Constant Fraction Discriminator, Gate and Delay Generator, and Universal Coincidence etc. Wave shapes from a scintillation detector, a high-purity Ge detector and the pulsing trigger will be directly recorded by the digital oscilloscope with a trigger from the coincidence module. Figure 2 shows a test result of 2D-AMOC spectrum for pure Fe measured by this system. The usual positron lifetime spectrum and the Doppler broadening energy spectrum are obtained by integrating with respect to the momentum and the time, respectively. On the other hand, the time dependent momentum distribution extracted from AMOC spectrum can give the chemical information on the positron trapping site every annihilation times, which is important to understand the correlation between precipitates and vacancy type defects.

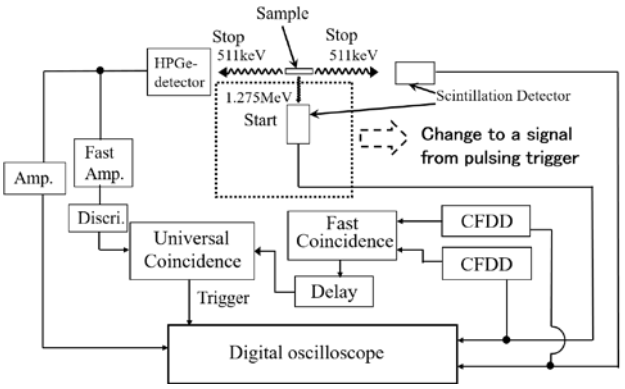

Figure 1: Schematic diagram of conventional 3 gamma AMOC; The start signal should be changed to pulsing trigger under the measurement using KUR positron beam.

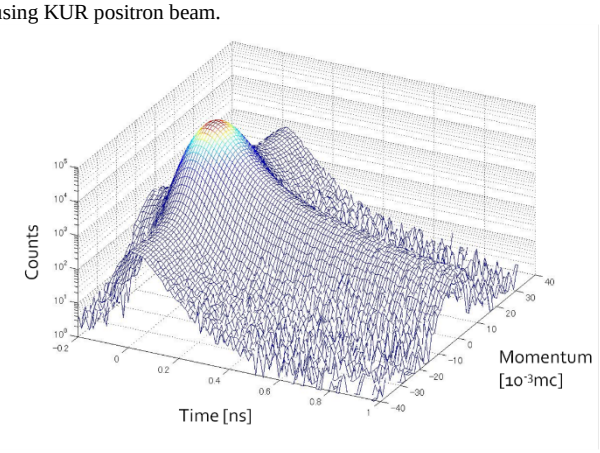

Figure 2: AMOC 2D spectrum of pure Fe.

We should develop and set up the beam bunching system which is consisted of the chopper, the pre-buncher and the buncher, and the brightness enhancement system which is consisted of a remoderator, some magnetic and electrical lenses. The AMOC measurement will be performed after restarting KUR.

REFERENCES:

[1] Q Xu *et al*, J. Phys. Conf. Ser. **505** (2014) 012030.
[2] K Sato *et al*, Nucl. Inst. Meth. Phys. Resear. B **342** (2015) 104.

CO4-5 Basic Study on Radiation-induced Luminescence from Natural Mineral

H. Fujita, M. Sakamoto[1]and T. Saito[1]

Nuclear Fuel Cycle Engineering Laboratories, JAEA
[1]Research Reactor Institute, Kyoto University

INTRODUCTION: It is well known that dielectric materials such as natural quartz exposed to ionizing radiation emit thermoluminescence (TL) and optically stimulated luminescence (OSL). OSL is a well-established tool for measuring radiation doses in unfired sediments [1]. It has features in common with TL which has long been used in measuring radiation doses [2]. Both TL and OSL dosimetry with white mineral do not need to be specially installed in advance, prior to dose estimation.

Quartz is an excellent material for use in dosimetry, because of its almost ubiquitous availability including an accidental place. Feldspar is an extensive ternary family of minerals appropriate for OSL and TL dosimetry as they display a strong luminescence and are quite common in the Earth's formation, although it has anomalous fading effects which decay OSL-related luminescence signals.

However, the detailed emission mechanisms of TL and OSL from natural minerals such as natural quartz and feldspar are not yet clear. In this study, the emission mechanisms of TL and OSL were investigated in conjunction with various radiation-induced phenomena after annealing treatments of quartz samples, involving TL, OSL and electron spin resonance (ESR) measurements.

EXPERIMENTS: Two surface soil samples were collected at different places in Ibaraki. Natural quartz samples were extracted from the soils by a usual treatment of 6M hydrochloric acid (HCl), 6M sodium hydroxide (NaOH) followed by 60 min of concentrated hydrofluoric acid (HF). The etching treatment with HF solution was at room temperature. Further purification of the quartz grains was performed by hand selection for the sake of elimination of feldspar grains as low as possible under a fluorescent lamp. The purified quartz samples were sieved to adjust the grain sizes ranging from 150 μm to 250 μm in a diameter for ESR spectrometry. The quartz samples were annealed at 800 ºC for 24 hours in an electric furnace, to make luminescence signals strong. The annealed quartz samples were irradiated a dose of 1 kGy with ^{60}Co source (0.64 kGy/h at D-30 cm) at room temperature at Kyoto University Research Reactor Institute (KURRI). The irradiated samples were stored at room temperature for one day to eliminate afterglow emission in a dark room. The ESR measurement was carried out using an ESR spectrometer (Jeol Ltd., JES-TE 200) at −196 ºC. Prior to the ESR measurements, the quartz samples were annealed for 1 min at 50 ºC intervals ranging from 150 to 300 ºC with a ceramic heater as preheat treatment. A part of each sample from two sampling points was kept in a dark room without preheating treatment. All preparations were carried out under dim red light.

After the ESR measurements, all samples were kept to measure luminescence signals in a dark room. However, an automated TL/OSL-reader system (JREC) had been improved to heat sample at correct temperature and then could not measure TL and OSL signals.

In this research, there were our two chances to do ESR experiment at the KURRI, but one of the chances was lost to measure ESR signals because the ESR spectrometer could not be worked in last August.

RESULTS: The ESR signals of Al centers as hole-trapped centers and Ti centers ($[TiO_4/H^+]^0$, $[TiO_4/Li^+]^0$ and $[TiO_4/Na^+]^0$) as electron-trapped centers were detected in the annealed quartz samples as before. ESR signal intensity of Al centers decreased with preheating temperatures, gradually. Finally, the ESR signals at 300 ºC of preheat were almost disappeared.

On the other hand, ESR signal intensity of Ti centers showed different tendency from the ESR intensity of Al centers. The intensity of Ti centers was constant up to 150 ºC of preheating temperature. After heating over 150 ºC, the intensity of Ti center decreased with preheating temperatures. Finally, the ESR signals at 300 ºC of preheat were almost disappeared as well as Al centers. The results agreed to our previous results. However, the intensity tendency of Ti centers was different between two quartz samples.

In this research, the luminescence emission mechanism could not be identified. Therefore, further work is necessary to identify luminescence mechanism using ESR measurement and annealing experiment. Moreover, the sample measured by ESR spectrometer should be used in luminescence measurement.

REFERENCES:

[1] Huntley, D. J., et al., Nature 313, 105-107 (1985).
[2] Mckeever, S. W. S., Cambridge University Press, Cambridge, 103-105 (1985).

CO4-6 Study of the Scientific Properties of Water and the Physiological Activation Phenomena by Using High-Intensity Pulsed Coherent Radiation

S. Okuda, Y. Tanaka, T. Kojima, S. Kurahashi, Y. Kida and T. Takahashi[1]

Graduate School of Engineering, Osaka Prefecture University
[1]Research Reactor Institute, Kyoto University

INTRODUCTION: The coherent transition radiation (CTR) from electron bunches of a linear accelerator (linac) has continuous spectra in a submillimeter to millimeter wavelength range. It is a picosecond pulsed light and hence, has extremely high peak-intensities compared with the other terahertz (THz) light sources. The light sources using the CTR have been applied to absorption spectroscopy [1-4]. However, such light sources are very limited. The light source system using the CTR from the electron beams of the 45 MeV L-band electron linac has been established at KURRI [5]. The CTR light source developed has been applied to absorption spectroscopy and it is expected that any nonlinear effects might be observed. Another important application is to the investigation of the biological effects of the CTR; few experiment has been performed so far.

The main purpose of the present work is the investigation of the biological effects of the high-intensity pulsed CTR.

CHARACTERISTICS OF THE CTR: The CTR is emitted as a pulsed and polarized radiation. The micropulse structure of the CTR corresponds to that of the electron beam from the linac. The light can produce the intense pulsed electric field and would cause some kind of excitation in a matter. The spectrum of the CTR is determined by the micropulse shape of the electron bunch whose pulse width is usually about 10 ps in the case of an L-band linac.

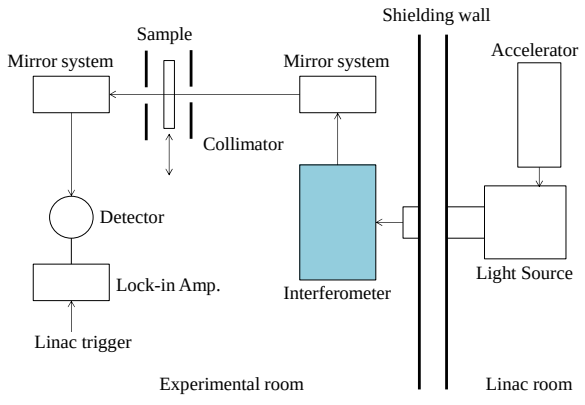

Fig. 1. Schematic diagram showing the configurations for absorption spectroscopy using the CTR

EXPERIMENTAL METHOD: The experimental configurations for the absorption spectroscopy are schematically shown in Fig. 1. The output CTR light from a light source chamber was transported out from the accelerator room. The spectrum of the light after passing through the sample was measured with a Martin-Puplett type interferometer and a liquid-He-cooled silicon bolometer. The sample was located on the light path between the interferometer and the detector. The light was focused at a light collimator 8 mmϕ in diameter located before the sample. The details of the methods for the measurements are described in ref. 5.

The liquid samples used in the experiments are water, aqueous solutions of NaCl, several kinds of bacillus, cell and microorganism. In the irradiation experiments of the CTR the sample holder shown in Fig. 2 was located just before the interferometer on the light path. The thickness of the liquid sample was about 100 μm, which was sandwiched with two anhydrous quartz plates 3 mm thick.

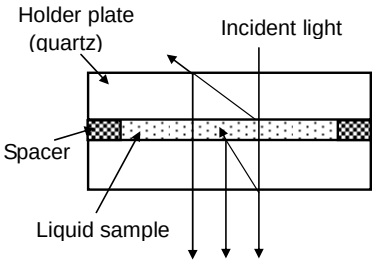

Fig. 2 Schematic diagram of the sample holder for liquid samples showing the behavior of the incident light.

RESULTS AND DISCUSSION: The basic properties of the CTR light source were investigated [6]. The light spectrum was sufficiently stable during the measurements within ±2-3% in a wavenumber range of 4-13 cm^{-1}. The range can be expanded to the lower or the higher wave numbers by using light filters. The wavenumber resolution was 0.1 cm^{-1}. The intensity of light was found to be sufficiently high even if it becomes 10^{-6} of the initial one after transmission through the sample due to absorption.

Some preliminary experiments to optimize the experimental conditions have been performed so far.

REFERENCES:

[1] T. Takahashi et al., Rev. Sci. Instrum. **69** (1998) 3770.
[2] K. Yokoyama, Y. Miyauchi, S. Okuda, R. Kato and T. Takahashi, Proc. 20th Int. Free-Electron Laser Conf. (1998, Williamsburg, USA) II 17-18.
[3] S. Okuda, M. Nakamura, K. Yokoyama, R. Kato and T. Takahashi, Nucl. Instrum. Meth. **A445** (2000) 267.
[4] S. Okuda et al., Radiat. Phys. Chem. **75** (2006) 903.
[5] S. Okuda and T. Takahashi, Infrared Phys. Technol. **51** (2008) 410.
[6] S. Okuda and T. Takahashi, J. Jpn. Soc. Infrared Science & Technology 25 (2016) 49 (in Japanese).

CO4-7 Analysis of Circularly Polarized CTR Using Babinet-Soleil Compensator

T. Takahashi

Research Reactor Institute, Kyoto University

INTRODUCTION: In recent years various types of coherent radiation emitted from a short bunch of relativistic electrons have attracted a considerable attention as a bright light source in the THz-wave and millimeter wave regions for the spectroscopic purpose. Coherent transition radiation (CTR), which is emitted from a boundary between two media, is one of such a coherent light source. CTR is usually utilized as a non-polarized light source, because the electric vector of transition radiation (TR) emitted from a metallic screen is axially symmetric with respect to the trajectory of an electron beam. In my previous reports [1] the circularly polarized CTR using a pair of wire-grid radiators with the different polarization has been developed with a new idea. Shibata *et al*. has developed a technique of generation of circularly polarized millimeter-wave radiation with the phase difference between the forward TR and the backward one [2]. However, it was difficult to control the polarization degree in that technique. The significant point of my new technique is the use of linearly polarized CTR with the wire-grid radiator. With this technique the polarization degree is able to be controlled precisely. In this report circularly polarized CTR has been analyzed using a hand-made Babinet-soleil compensator. Circularly polarized light has been useful in the circular dichroism spectroscopy.

EXPERIMENTAL PROCEDURES: The experiment was performed at the coherent radiation beamline [3] at the L-band linac of the Research Reactor Institute, Kyoto University. The energy, the width of the macro pulse, and the repetition rate of the electron beam were 42 MeV, 33 ns, and 20 Hz, respectively. The average current of the electron beam was 0.5 μA. The schematic diagram around the radiation source of this experiment is shown in Fig.1. Two wire-grid polarizers (WG1 and WG2) 10 μm thick with 25 μm spacing were used in order to generate the CTR with horizontal and vertical components, respectively. Each CTR was superposed with phase difference through the optical delay system. Although a Martin-Puplett-type interferometer is usually used as a spectrometer, a grating-type monochromator was used in this experiment. The monochromator was set for the wavelength of 2.3 mm. The CTR was detected by a liquid-helium-cooled Si bolometer. In order to measure the polarization diagram a wire-grid polarizer with a rotary holder and a Babinet-soleil compensator were used in front of the detector.

RESULTS: The observed polarization diagrams of circularly polarized CTR at the phase difference of π/2 and 3π/2 are shown in the left figures in Figs.1 and 2, respectively. In order to analyze the circular polarization the thickness of the Babinet-soleil compensator was set as a quarter-wave retarder. The observed light through the compensator has not perfect linear polarization as shown in the right figures in Figs.1 and 2. These results have been attributed to the lack of coherence of CTR because of the large size of the electron beam.

REFERENCES:

[1] T. Takahashi, *et al.*, KURRI-PR 2014 CO4-15.
[2] Y. Shibata *et al.*, Rev. Sci. Instrum. **72** (2001) 3221.
[3] T. Takahashi *et al.*, Rev. Sci. Instrum. **69** (1998) 3770.

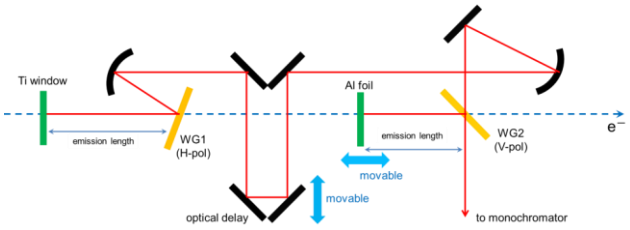

Fig.1. The schematic diagram of the experiment.

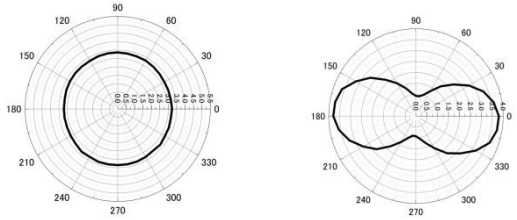

Fig.2. Circularly polarized CTR at the phase difference π/2 (left) and polarization diagram through the compensator (right).

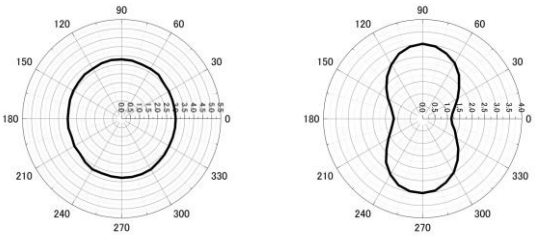

Fig.3. Circularly polarized CTR at the phase difference 3π/2 (left) and polarization diagram through the compensator (right).

CO4-8 ^{57}Fe Mössbauer Spectra of Normalconducting $Sr_2CrFeAsO_{3-d}$

T. Otsuka, H. Fujioka, M. Matoba, S. Kitao[1], M. Seto[1] and Y. Kamihara
Department of Applied Physics and Physico-Informatics, Keio University
[1]*Research Reactor Institute, Kyoto University*

INTRODUCTION: Layered oxypnictide $Ae_2T_MFePnO_{3-d}$ (Ae = Alkaline earth metal, TM = Transition metal) (21113) consists of carrier conducting Fe*Pn* (*Pn* = P and As) layer and carrier blocking $Ae_2T_MO_3$ layer. Several 21113 shows superconducting phase at low temperatures. Hyperfine fields (B_{hf}) measurements experienced by nuclei of atoms at crystallographic sites in magnetic and/or antiferromagnetic metals are of interest in view point of hyperfine interactions and important for their use in the determinations of nuclear magnetic dipole moments by a variety of methods including those based on low-temperature nuclear orientation. Guang-Han Cao et al reported that $Sr_2VFeAsO_{3-d}$ is an FeAs-based layered oxypnictide superconductor, which reveals antiferromagnetic under 150 K originating in local d-electron moments of vanadium, and the superconducting transition temperature T_c is 24 K.[1] In this study, we focus on magnetic phase of $Sr_2CrFeAsO_{3-d}$ as a possible mother compound of iron-based superconductors. [1-5]

Element-specific magnetism and electronic phase of Fe sublattice in $Sr_2CrFeAsO_{3-d}$ are elucidated using ^{57}Fe Mössbauer spectroscopy. Studies on hyperfine fields B_{hf} experienced by nuclei of impurity phases are of interest in view point of hyperfine interactions and important for their use in the determinations of nuclear magnetic dipole moments by a variety of methods including those based on low-temperature nuclear orientation.

EXPERIMENTS: Polycrystalline samples of $Sr_2CrFeAsO_{3-d}$ were prepared by the solid-state reactions in a sealed silica tube using dehydrated SrO, FeAs, Cr_2O_3, Cr as starting materials. Then, a mixture of the three powders was pressed into pellet and heated in doubly sealed silica tubes at 1030~1330 °C for 40 h. All procedures were carried out in an Ar-filled glove box (MIWA Mfg; O_2, H_2O < 1 ppm). The crystal phase of the obtained product was examined by powder X-ray diffraction (XRD; RigakuRINT-2500) using CuKα radiation. Almost all the diffraction peaks are assigned to the $Sr_2CrFeAsO_{3-d}$ phase. Electrical resistivity measurements were performed at 2–300 K by a dc four-probe technique using silver paste as electrodes. Magnetization measurements were performed for polycrystalline samples using a Quantum Design magnetic properties measurement system (MPMS). The ^{57}Fe Mössbauer (MS) experiment on the two series of compounds, $Sr_2CrFeAsO_{3-d}$ (x = 0.03, 0.18) was performed with conventional ^{57}Fe MS equipment using 14.4 keV γ-rays from a ^{57}Co source in an Rh matrix.

RESULTS: ^{57}Fe MS to the samples of d=0.03, 0.18 of $Sr_2CrFeAsO_{3-d}$ were measured and analyzed for obtaining quantitative value of internal magnetic field. As a result, the existence of spin density wave phase are observed for x = 0.18, while antiferromagnetic ordered Fe are observed for x = 0.03. The result indicates that normalconducting $Sr_2CrFeAsO_{3-d}$ shows two magnetic ground states, which stabilities depend on oxygen deficiency.

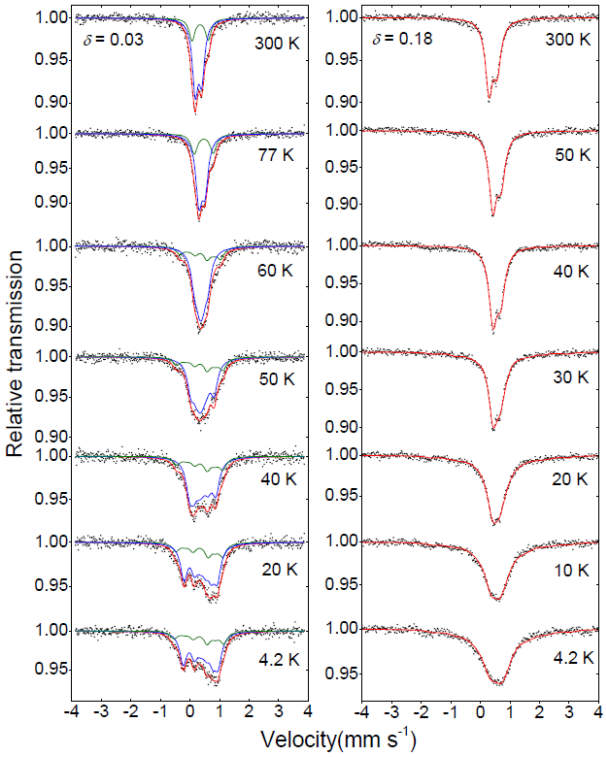

Fig. 1. ^{57}Fe Mössbauer spectra (MS) of polycrystalline $Sr_2CrFeAsO_{3-d}$ (d = 0.03 and 0.18) at several temperatures described in the figure. The solid lines for d = 0.03 are fitted patterns provided that a internal magnetic field. The solid lines for d = 0.18 are fitted patterns provided that a wide distribution of internal magnetic field. Profiles of FeAs, which are denoted by Green lines, are reproduced from Blachowski et al's results. [6,7]

REFERENCES:

[1] G. H. Cao et al., Phys. Rev. B 82, 104518 (2010).
[1] Y. Kamihara et al., New J. Phys. 12, 033005 (2010).
[2] D. Johrendt et al., Physica C, 469, 9 (2009).
[3] X. Zhu et al., Phys. Rev. B 79, 220512 (2009).
[4] M. Tegel et al., Z. Anorg. Allg. Chem. 635, 2242 (2009).
[5] X. Zhu et al., Sci. China Ser. G 52, 1876 (2009).
[6] A. Blachowski et al., J. Alloy. Compd. 582, 167 (2014).
[7] A. Blachowski et al., Phys. Rev. B 83, 134410 (2011).

CO4-9 Complex Structure of Ions Coordinated with Hydrophilic Polymer. 16. Application for Metaric Plating on Resin Surface. (1)

A. Kawaguchi and Y. Morimoto

Research Reactor Institute, Kyoto University

INTRODUCTION: We have reported interacted structures between iodine (polyiodide ions, I_n^{m-}, *m*, *n*: integer, $n \neq 1$) and polymers.[1] While polyiodide ions (and their counter-ions) are prepared as solutes in aqueous solution, they can be diffused into various polymeric matrix. Such structures and procedures are expected to introduce novel functionality and wide applications to polymeric materials with easy operation.[2]
For some hydrophilic polymers, diffusion of iodine from aqueous solutions advances very quickly and, in some matrix such as polyamide-6 (PA6), ionic diffusion into crystallite region or "diffusion-induced" orientation are also observed through easy operation at room temperature; as phenomena, iodine-doped polymers can be regarded as "pseudo solvents" for ionic diffusion.[3,4]
These results suggest that coordination between iodine and polymers is dynamic and pliable and activated process and that previous existence of polyiodide ion drastically enhances posterior ionic diffusion in polymers. On the other hand, self-organization and diffusion keeping ordered structure are also observed; processes looked opposite or paradoxical go simultaneously as both ordering and disordering effects. Furthermore, such ionic behavior can be qualitatively applicable for hydrophobic matrix even if sample operation are wholly carried out with aqueous solution of polyiodide ions.[5]
Some advantages can be suggested as availability for such operation using polyiodide ions: maintenance of shape or convenience of size of matrix, deep and gradient injection of inorganic components in spite of operation even at room temperature, preparation with aqueous solutions,,, etc. Previously, we reported "(1st) iodine doping" and "secondary doping" of Ag^+ ion into hydrophobic materials with aqueous solutions.[6] Here, injection of metallic ions or inorganic salts into polymeric matrix are expected to apply electroless plating resin surface.

EXPERIMENTS: As hydrophobic materials as matrix, silicone-rubber tube (LABORAN, ϕ2x4), PE (polyethylene) tube and PP (polypropylene) film were treated. These matrixes were "iodine doped" by immersing in I_2-KI(aq) or I_2-NH_4I(aq) (3.0N) for more than one week. For secondary doping of Ag^+ ion, each samples were immersed in $AgNO_3$(aq) (2.0M) solution for a few days. On electroless plating of Cu in aqueous solution, THRU-CUP PSY (UYEMURA) was used. All opera-tion were done at room temperature (c.a. 25℃).

RESULTS: Intrinsically, the treated three matrixes are hydrophobic as chemical composition. Actually, affinity with each aqueous solutions was not so activated in each process without "iodine doping". And, even applying "iodine doping", increase in mass (Δm) in each preparation steps were tiny (less than 1-2%) and colored appearance on "(1st) iodine doping" was negligibly slight while, to hydrophilic matrixes, Δm = 50-200% (or more) or solid and tough "black" coloring were frequently observed for "iodine doping".[1] However, as results after electroless Cu plating process to the hydrophobic matrixes, deposition of Cu was observed on surface of each hydrophobic matrixes.(Figure)
Such Cu deposition is regarded as process at restricted surface region of each matrixes. In the cases of hydrophobic matrixes, diffusion of polyiodide ions might be qualitatively very slight and following ionic diffusion introduced posteriorly is also negligible; ionic diffusion and exchange (ex. polyiodide ions, counter ions, "secondarily doped" ions,,,) are hardly explicit like as hydrophilic systems. Nevertheless, results showing activated affinity with aqueous solutions means that "iodine doping" can suggest potential abundance for functionality to unexpected matrixes.

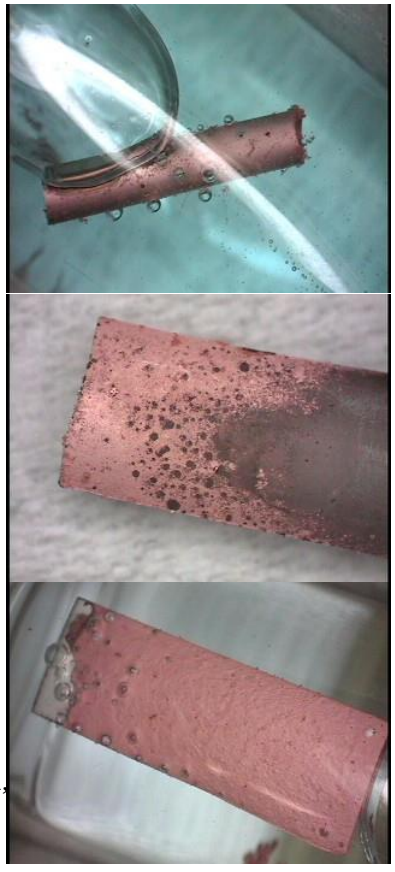

Figure: Electoless plating for hydrophobic matrixes treated with aqueous solutions for all process after applying polyiodide: silicone rubber tube (top), PE tube (center), PP film (bottom).

REFERENCES:

[1] A. Kawaguchi, Polymer, **35**, 3797-3798. (1994)
[2] patent. JPN -5444559 (2014).
[3] KAWAGUCHI Akio, et.al., SPring-8 User Exp. Rep. **5** (2000A), 354-354. (2000)
[4] A. Kawaguchi, Polym. Prep. Jpn., **62**, 5116-5117. (2013)
[5] A. Kawaguchi, Polym. Prep. Jpn., **64**, (3H07) (2015)
[6] Y. Gotoh, *et.al.*, Polym. Prep. Jpn., **51**, 2259-2259. (2002)

CO4-10 Interactions of Deuterium with Defects Created in Tungsten by Irradiation of High Energy Electrons

Y. Hatano, K. Ami[1], T. Toyama[2], K. Sato[3] and Q. Xu[4]

Hydrogen Isotope Research Center, Organization for Promotion of Research, University of Toyama
[1]Graduate School of Science and Engineering for Education, University of Toyama
[2]Institute for Materials Research, Tohoku University
[3]Graduate School of Science and Engineering, Kagoshima University,
[4]Research Reactor Institute, Kyoto University

INTRODUCTION: Retention of hydrogen isotopes especially tritium in plasma facing materials is one of the important issues in safety assessment of fusion reactors. Recent report shows that neutron irradiation significantly increases deuterium (D) retention in W, a leading candidate of plasma-facing material, due to trapping effects of radiation-induced defects [1]. However, detailed trapping mechanisms have not been clarified. For better understanding of defect-hydrogen isotope interactions, in this study, W specimens were irradiated with high energy electrons to induce Frenkel pairs uniformly throughout the bulk, and clustering of vacancy-type defects and D trapping were examined using positron annihilation spectroscopy (PAS) and thermal desorption spectroscopy (TDS).

EXPERIMENTS: Disks of recrystallized W (RC-W) and stress-relieved W (SR-W) were irradiated with 8.5 MeV electrons at around 373 K to 10^{-3} dpa. Then those specimens were subjected to exposure to D_2 gas (0.1 MPa) or annealing in vacuum at 573 K for 100 h. Size distributions of vacancy-type defects were examined using PAS, and D retention was measured using TDS.

RESULTS AND DISCUSSION: The results of positron lifetime measurements for RC-W are summarized in Table 1. The positron lifetime before the irradiation was 118 ps. It clearly increased to 170 ps by the electron irradiation due to formation of dislocations, mono- and/or divacancies. Long lifetime components appeared after D_2 gas exposure and annealing in vacuum at 573 K, and the positron lifetime after D_2 gas exposure (~280 ps) was significantly shorter than that after annealing in vacuum (~342 ps). The increase in positron lifetime showed the clustering of vacancies. The difference between D_2 gas exposure and annealing in vacuum can be explained by retardation of clustering of vacancies by D in W and/or decrease in the effective open-volume in vacancy clusters due to D trapping. Similar change in the lifetime was observed also for SR-W. Coincidence Doppler broadening spectroscopy showed that the correlations between S and W parameters for the specimens before irradiation, after irradiation and after annealing in vacuum fell on a single straight line in S-W plot, while the specimen exposed to D_2 gas after the electron irradiation showed the clear deviation from the line. These observations are good evidences for that D was trapped at vacancy clusters.

TDS showed significant increase in D retention due to the irradiation, as shown in Fig. 2; D concentration in RC-W increased from [D]/[W] = 1.1×10^{-6} to [D]/[W] = 8.6×10^{-6}. A desorption peak appeared at 850 K and a shoulder was observed at 975 K. These two desorption stages appeared to correspond to the detrapping of D from small and large vacancy clusters observed using PAS. The evaluation using a diffusion analysis program showed that these desorption temperatures correspond to the activation energy for detrapping of 1.55 and 1.85 eV. Interestingly, D retention in the irradiated SR-W was larger than that in the irradiated RC-W and it was [D]/[W] = 5.5×10^{-5}.

Table 1 Positron lifetime in W under as-prepared conditions (non-irr.), after electron irradiation at ~373 K to 10^{-3} dpa (e-irr.) and subsequent annealing at 573 K for 100 h in vacuum (e-irr. vac. anneal.) and in 0.1 MPa D_2 gas (e-irr. D_2 exp.).

Sample		non-irr.	e-irr.	e-irr. vac. anneal.	e-irr. D_2 exp.
Positron life time (ps)	Average	118	170	231	194
	Short life component	-	-	130	134
	Long life component	-	-	342	280

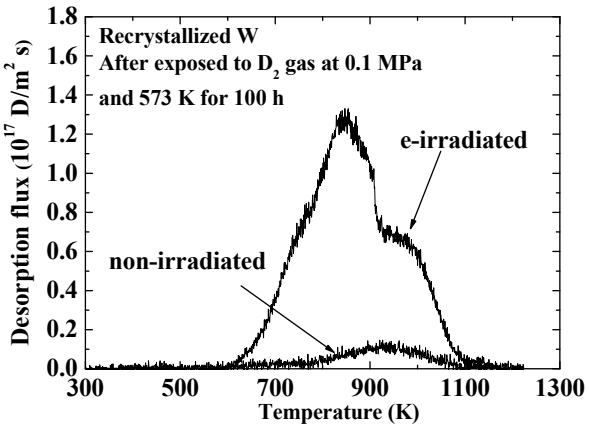

Fig. 2 Thermal desorption spectra of D from the recrystallized W specimen under as-prepared conditions and that irradiated with 8.5 MeV electrons to 10^{-3} dpa.

REFERENCES:

[1] Y. Hatano *et al.*, J. Nucl. Mater., **438** (2013) S114–S119 and Nucl. Fusion **53** (2013) 07300

CO4-11 Effect of Ion Species on Defect Formation near Surface of GaSb by Ion Irradiaiton

C. Watanabe, N. Nitta, M. Taniwaki, A. Kinomura[1] and T. Yoshiie[1]

School of Environmental Science and Engineering, Kochi University of Technology
[1]Research Reactor Institute, Kyoto University

INTRODUCTION: Porous structure is formed on GaSb surface by ion beam irradiation [1], [2]. It was clarified that the structure is formed by migration of point defects induced by ion irradiation. The first the voids form from the oversaturated vacancies and they develop by movement of vacancies and interstitials. However, the the detailed process of void formation has not yet been understood. In this study, the effect of various ion species on GaSb void formation by ion irradiation was investigated. The ion species used in this work are ions of carbon group elements, by which it will be possible to detect only the effect of ion mass except the chemical effect.

EXPERIMENTS: GaSb (001) wafers were irradiated at about 100 K by C, Si, Ge, Sn, Pb using a heavy ion accelerator at Research Reactor Institute, Kyoto University. The acceleration voltage was 60 kV. The ion dose was 2.80×10^{19} ions/m^2 for C, 1.57×10^{19} ions/m^2 for Si, 1.01×10^{19} ions/m^2 for Ge, 6.02×10^{18} ions/m^2 for Sn, and 7.05×10^{18} ions/m^2 for Pb. These ion doses were determined to gives a same peak concentration in depth profile of vacancy concentration in GaSb calculated by SRIM code simulation [3], adopting the displacement threshold energy values obtained by Thommen (6.2 eV for Ga and 7.5 eV for Sb) [4]. The surface morphology was observed by a FE-SEM (field emission scanning electron microscope, JEOL JSM-7401F).

RESULTS AND DISCUSSION: The voids were observed on the surfaces irradiated by relatively large mass ions (Ge, Sn, and Pb), and they were scarcely formed on the surfaces irradiated by the small mass ions (C and Si). Figure 1 shows distributions of vacancy created by one ion irradiation obtained by SRIM code simulation. The distribution of point defects in depth direction is much different between ion species. In the case of light ions, vacancies are formed in deep region from the surface and the local vacancy concentration is low. In the case of heavy ion, the vacancies are created in shallow region and its local concentration is high, when they aggregate easily and lead to void formation. In contrast, vacancies created at low concentration in wider region diffuse so that void formation scarcely occurs. This is the explanation that the surface structures were different between heavy ion irradiation (Ge, Sn and Pb) and light ion irradiation (C and Si).

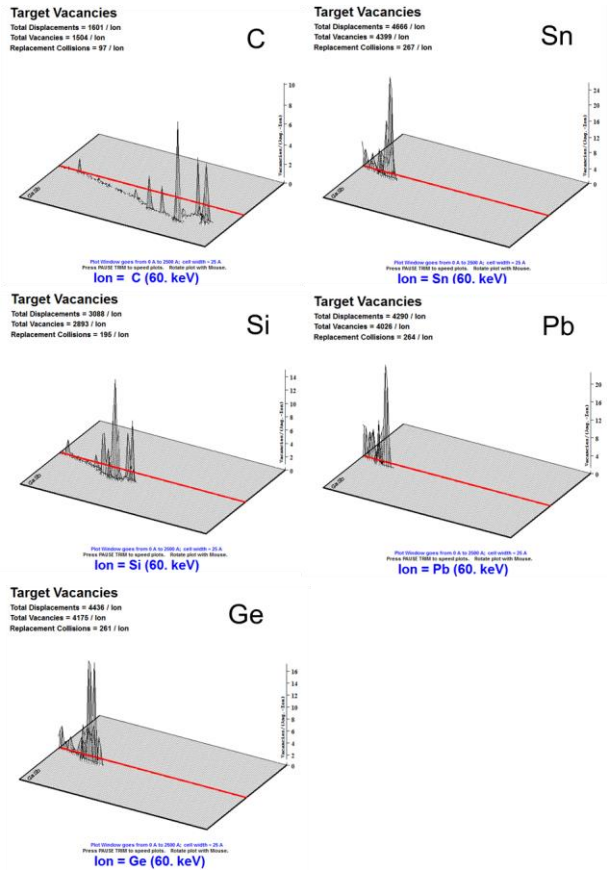

Fig. 1. Vacancy distributions of one ion irradiation obtained by SRIM code simulation.

REFERENCES:

[1] D. Kleitman and H. J. Yearian, Phys. Rev. 108 (1957) 901.
[2] N. Nitta, M. Taniwaki, Y. Hayashi and T. Yoshiie, J. Appl. Phys., 92 (2002), 1799-1802.
[3] J. P. Biersack and L. G. Haggmark, Nucl. Instrum. Methods 174, (1980) 257; J. Ziegler, Software and web site, http://www.SRIM.org.
[4] D. Thommen, Phys. Rev. 174, (1968) 938.

CO4-12 Electron Beam Test of Avaranche Photodiode for Ganymede Laser Altimeter of Jovian Icy Satellite Exploerer

M. Kobayashi, O. Okudaira, K. Ishibashi, M. Fujii[1], T. Takahashi[2] and N. Abe[2]

Planetary Exploration Research Center, Chiba Institute of Technology
[1]FAM science
[2]Research Reactor Institute, Kyoto University

INTRODUCTION: The Ganymede Laser Altimeter (GALA) as part of the JUICE (Jovian Icy Satellite Explorer) payload is one of the instruments focusing on aspects related to the presence and characterizations of subsurface water oceans [1] [2]. For the first time the time-variability of the global figure of a moon due to tides exerted by Jupiter will be detected by altimetry measurements.

Laser pulses are emitted at a wavelength of 1064 nm by using a Q-switched Nd:Yag laser at operational frequencies of 30 and 75 Hz, respectively. The pulse energy and pulse repetition frequency depend on the different JUICE mission phases. The beam is reflected from the surface (surface spot size is about 50 m) and received around 3 ms (assuming the 500 km orbit) later at a 25 cm diameter F/1 telescope. The returning laser pulse is refocused onto a silicon avalanche photodiode (or APD) through a narrow bandpass interference filter. The signal is then sampled and fed to a digital range finder. This system determines the time of flight (and therefore range), the integrated pulse intensity, its width and full shape. The data are passed to a digital processing unit which controls the operation and services the spacecraft interface. GALA will provide <1 ns time resolution (<15 cm range, <8 cm under optimal conditions).

APD for GALA: We adopted an APD product manufactured by Excelitas Technologies, Montreal in Canada. They commercially manufacture APD product particularly a hybrid module of APD which contains an APD sensor, a preamplifier, a thermo-electric controller and a temperature sensor in a package. Their APD product that are customized for space use have been adopted for space missions due to its compactness and heritage in space.

The APD has also sensitivity to radiation that induces hole-electron pair in the depression layer. In space environment, the induced signal may affect light detection as background noise, called radiation noise. Jupiter has a strong magnetosphere and previous studies revealed energetic electrons are trapped in the magnetosphere and major component among the other ionizing radiation like proton and the other energetic ion. The APD will be shielded up against to the Jovian radiation environment however some of electrons can penetrate the shield into the APD. In this study, we used KURRI-LINAC as an electron beam source to emulate electrons irradiating the APD to investigate how energetic electron induces signals and interferes the returning laser pulse signal.

EXPERIMENTS: We used an APD product of C30954E, Excelitas Technologies, which is the same product as one for GALA. The APD sensor has a diameter of 0.8 mm and an enhanced sensitivity in infrared range, about 0.4 of quantum efficiency at 1064 nm. It does not include any preamplifier so a preamplifier was prepared and externally attached to the device. The amplifier is a trans-impedance amplifier, the same as one for GALA flight APD. Although the band width for GALA APD had not been decided yet, 100 MHz was adopted as plausible number for the GALA APD.

In an irradiation test, 5 MeV electron were irradiated to the APD. During irradiation, reverse bias high voltage was applied to the APD sensor and the ground line was fed to the following preamplifier. The output signals of the amplifier were monitored and recorded with a digital oscilloscope.

RESULTS: As shown in Fig. 1, clear pulse signals were detected and they correspond to vertical hits of single electron on the APD sensor. In actual environment, energetic electron with various energies omni-directionaly comes and penetrates the sensor. And also the APD sensor will be sit in the radiation shield where secondary radiation are induced affecting the optical returning pulses. Those will be investigated in further experiments.

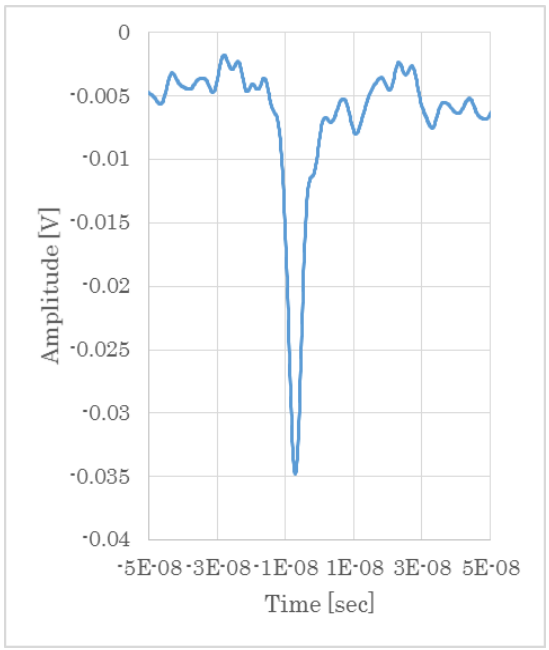

Fig.1. An example of output signal pulse from the APD.

REFERENCES:

[1] H. Hussman *et al.*, EPSC Abstracts, vol. 8, EPSC2013-428, 2013.
[2] H. Hussman *et al.*, EPSC Abstracts, vol. 9, EPSC2014-347, 2014